

FROM NUCLEI TO STARS WITH A TROJAN HORSE*

A. TUMINO^{a,b}, C. SPITALERI^{a,c}, M. LA COGNATA^a, M.L. SERGI^{a,c}
S. CHERUBINI^{a,c}, M. GULINO^{a,b}, L. LAMIA^c, R.G. PIZZONE^{a,c}
S.M.R. PUGLIA^a, G.G. RAPISARDA^{a,c}, S. ROMANO^{a,c}, R. SPARTÁ^a

^aLaboratori Nazionali del Sud — INFN, Catania, Italy

^bUniversità degli Studi di Enna “Kore”, Enna, Italy

^cDipartimento di Fisica e Astronomia — Università di Catania, Catania, Italy

(Received November 19, 2013)

Nuclear reactions are responsible for the energy production in stars and related nucleosynthesis processes. For this reason, an accurate knowledge of their rates at the energies of interest is required. The Trojan Horse Method has been introduced to overcome the experimental difficulties arising from the small cross sections involved in reactions induced by charged particles at astrophysical energies. This is done by measuring the quasi-free cross section of an appropriate three body process. The basic theory of the Trojan Horse Method will be presented together with a review of some recent experimental results.

DOI:10.5506/APhysPolB.45.181

PACS numbers: 24.50.+g, 24.10.-i, 25.70.Hi, 26.20.-f

1. Introduction

The interconnection between macro- and micro-cosmos has been officially established in the famous B²FH paper [1], considered as the greatest gift of nuclear astrophysics to modern civilization. In particular, the elements composing everything, from planets to life, were forged inside earlier generations of stars, and nuclear reactions are responsible for both energy production and creation of the elements. It becomes thus important to determine their reaction rates down to the energy range of astrophysical importance, that for charged particles is represented by the so-called “Gamow peak” [2]. The Gamow peak is the result of the convolution of the higher energy tail of the Maxwell–Boltzmann distribution, describing the velocity of the nuclei in the stellar plasma, and of the Gamow factor, $\exp(-2\pi\eta)$, that is a good approximation of the penetration factor through the Coulomb barrier at such low energies. This is the region where the measurement should be carried out,

* Presented at the XXXIII Mazurian Lakes Conference on Physics, Piaski, Poland, September 1–7, 2013.

but it is usually far below the Coulomb barrier of the interacting nuclei. Because of that, the cross section $\sigma_b(E)$ of these reactions drops exponentially with decreasing center-of-mass energy: $\sigma_b(E_{\text{cm}}) \sim \exp(-2\pi\eta)$, where η is the Sommerfeld parameter, $\eta = Z_1 Z_2 / (hv)$, depending on the charge numbers Z_1, Z_2 of the colliding nuclei and on their relative velocity v in the entrance channel. This makes the direct experiments challenging and the standard way to proceed is to measure the cross section over as wide a range as possible, then extrapolate down to the Gamow peak using the definition of the astrophysical factor, as given by

$$S_b(E) = E\sigma_b(E) \exp(2\pi\eta) \quad (1)$$

which is a smoothly varying function of the energy than the cross section, with the inverse of the Gamow factor introduced to remove the dominant energy dependence of the bare nucleus cross section $\sigma_b(E)$ due to the barrier penetrability. However, extrapolation can be a source of additional uncertainty due, for example, to unknown resonances or tails of sub-threshold resonances at stellar thermonuclear energies that can be missed [2, 3].

In addition, the few accurate direct measurements close to the Gamow peak experience the electron screening effect due to the electrons surrounding the interacting ions [4]. Electron screening acts in a way to produce an enhancement of the cross section at ultra-low energy, thus preventing one to measure the bare nucleus cross section. The cross section rise is usually parameterized by means of the so-called screening factor

$$f_{\text{lab}}(E) = \sigma_s(E)/\sigma_b(E) \sim \exp(\pi\eta U_e/E) \quad (2)$$

with $\sigma_s(E)$ and $\sigma_b(E)$ the cross sections of shielded and bare nuclei, respectively, and U_e the electron screening potential energy.

One has to notice that laboratory screening is different from that in stellar plasma, thus the relevant parameter to evaluate correctly the reaction rate is σ_b . Obviously, one needs to know U_e to access σ_b from the experimental σ_s . However, experimental studies of reactions involving light nuclides have shown that the observed exponential enhancement of the cross section at low energies were in all cases significantly larger (about a factor of two) than it could be accounted for from available atomic-physics model using the adiabatic limit of U_e . This means that in spite of the several efforts, σ_b (or equivalently $S_b(E)$) cannot be measured at the Gamow peak, rather its behavior has to be extrapolated from the higher energies, usually with the help of theoretical arguments. To overcome all these experimental difficulties, indirect methods [5] such as the Coulomb Dissociation [6], the Asymptotic Normalization Coefficients [7], and the Trojan Horse Method (THM) [8–14] have been developed in the last twenty years. They make it

possible not only to measure cross sections at never reached energies but also to determine the electron screening potential when direct data are available at those energies. Here, we recall the basic ideas of the THM together with some recent results.

2. Basic ideas of the Trojan Horse Method

The THM makes use of the quasi-free (QF) contribution of an appropriate $A + a \rightarrow C + c + s$ three-body reaction, the Trojan Horse (TH) reaction, performed at energies well above the Coulomb barrier to extract the cross section of a charged particle $A + x \rightarrow C + c$ two-body reaction [8] at astrophysical energies free of Coulomb suppression [15, 16]. The scientific background of the THM is in the theory of QF reaction mechanisms. Its application to nuclear astrophysics is an extension to the low energies of two decades of well assessed higher energy QF measurements [17, 18]. In particular, the THM has been successfully applied to determine the bare nucleus cross section of several reactions between charged particles of astrophysical relevance (see Table I for relevant references). Besides, several tests have been performed to explore the full capabilities of the method: the possible use of virtual neutron beams to study neutron induced reactions on stable [20, 21] and in the future on radioactive nuclei; the spectator invariance of the reaction amplitude for the two-body reaction of interest, comparing results obtained from ^2H and ^3He break-up [22, 23] and from ^6Li and ^3He break-up [24, 25, 37].

The first assumption of the THM is that nucleus a is described in terms of the $x \oplus s$ cluster structure. In many applications [15, 32, 39, 44, 46], this is trivially fulfilled: $a = \text{deuteron}$, $x = \text{proton}$, $s = \text{neutron}$. The energy for the $A + a$ relative motion is chosen to be above the Coulomb barrier in such a way that the two body interaction can be considered as taking place inside the nuclear field, without experiencing either Coulomb suppression or electron screening effects. The $A + a$ relative motion is compensated for by the $x-s$ binding energy, determining the so-called “quasi-free two-body energy” given by

$$E_{\text{qf}} = E_{Aa} - B_{x-s}, \quad (3)$$

where E_{Aa} represents the beam energy in the center-of-mass system and B_{x-s} is the binding energy for the $x-s$ system. In Eq. (3), E_{qf} is not changed varying the projectile energy. What is done is to keep the beam energy at a fixed value and to vary the relative momentum p_{xs} from its QF value to an upper limit given by $\kappa_{xs} = \sqrt{2\mu_{xs}B_{xs}}$ that represents the on-energy-shell (OES) $a = (xs)$ bound state wave number [26]. This upper limit is usually few tens of MeV/ c . This little variation is linked to the $x-s$ intercluster motion inside a and it is taken on the p_s variable, the momentum of the

spectator particle (in the laboratory system $\vec{p}_{xs} = \vec{p}_x = -\vec{p}_s$) and/or on its emission angle, both measured or easily reconstructed. This brings to the following formula

$$E_{\text{QF}} = \frac{m_x}{m_x + m_A} E_A - \frac{p_s^2}{2\mu_{xs}} + \frac{\vec{p}_s \cdot \vec{p}_A}{m_x + m_A} - B_{xs}. \quad (4)$$

Thus, the cutoff in the momentum distribution fixes the range of energies around the “quasi-free two-body energy” accessible in the astrophysical relevant reaction. In the Impulse Approximation either in Plane Wave or in Distorted Wave (this does not change the energy dependence of the two-body cross section but only its absolute magnitude), the three-body cross section can be factorized as

$$\frac{d^3\sigma}{dE_c d\Omega_c d\Omega_C} \propto [\text{KF} |\varphi_a(\mathbf{p}_{sx})|^2] \left(\frac{d\sigma}{d\Omega_{\text{cm}}} \right)^{\text{HOES}}, \quad (5)$$

where KF is a kinematical factor containing the final state phase-space factor. It is a function of the masses, momenta and angles of the outgoing particles [39]; $\varphi_a(\mathbf{p}_{sx})$ is proportional to the Fourier transform of the radial wave function $\chi(\mathbf{r})$ for the x - s inter-cluster relative motion; $(d\sigma/d\Omega_{\text{cm}})^{\text{HOES}}$ is the half-off-energy-shell (HOES) differential cross section for the binary reaction at the center-of-mass energy E_{cm} determined from the relative energy of the outgoing particles c and C , the decay products of the virtual two-body reaction of interest, once their energies are measured

$$E_{\text{cm}} = E_{cC} - Q_{2b}. \quad (6)$$

Q_{2b} is the Q -value of the binary reaction.

Equation (5) can be provided by a schematic pole diagram with two vertices, shown in Fig. 1. In the upper vertex, a breaks up into its components, while the lower vertex refers to the two-body reaction of interest that takes place once x is transferred.

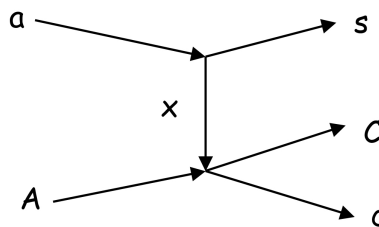


Fig. 1. Diagram representing the quasi-free $A + a \rightarrow C + c + s$ reaction; nucleus A interacts only with cluster x , leaving particle s as a spectator to the process.

In a typical THM experiment, nuclei c and C are detected and identified by means of telescopes (silicon detector or ionization chamber as ΔE step and position sensitive detector as E step) placed at the so-called quasi-free angles. High energy and angular resolutions are required and typical values are of the order of 1%. A number of steps are involved in the data analysis before the two-body cross section of astrophysical relevance can be extracted. These steps include:

1. identification of events belonging to the $A + a \rightarrow C + c + s$ three-body reaction of interest;
2. tests of the QF mechanism and selection of QF events;
3. extraction of the $A + x \rightarrow C + c$ two-body cross section, $\sigma_b(E)$, from the measured three-body one in arbitrary units; the two-body cross section below the Coulomb barrier needs to be corrected for the penetrability;
4. normalization procedure to obtain $\sigma_b(E)$ in absolute units;
5. validity tests to verify that direct data are reproduced both in the excitation function, including resonances, and in the angular distributions;
6. evaluation of the electron screening potential when direct measurements are available at ultra-low energies.

After the selection of the reaction channel, the most critical point is to select the quasi-free mechanism, often overlapping with other reaction mechanisms feeding the same particles in the final state, *e.g.* sequential decay and direct break-up. An observable which is very sensitive to the reaction mechanism is the shape of the experimental momentum distribution of the spectator, $|\varphi(\mathbf{p}_{xs})|^2$. It is determined using a standard procedure applied to each pair of coincidence detectors that selects the coincidence yield in narrow relative energy windows, ΔE 50 to 100 keV, and center-of-mass angular range $\Delta\theta_{\text{cm}}$ 0.5 to 2°, where $\frac{d\sigma}{d\Omega_{\text{cm}}}$ ^{HOES} can be considered constant. Thus, the momentum distribution can be retrieved simply dividing the coincidence yield by the kinematical factor

$$|\varphi(\mathbf{p}_{xs})|^2 = \frac{Y_d}{\text{KF}}. \quad (7)$$

The extracted experimental momentum distribution is then compared with the theoretical one that in Plane Wave Impulse Approximation (PWIA) represents the Fourier transform of the radial x - s bound state wave function. To check if the simple PWIA approach gives an accurate description of the momentum distribution, the Distorted Wave Born Approximation (DWBA) distribution is usually evaluated also by means of the FRESKO code [27], with optical potential parameters taken from the Perey and Perey compilation [28]. A comparison between the two behaviors and the experimental

momentum distribution is shown in Fig. 2 referring to the study of the $^{17}\text{O}(p, \alpha)^{14}\text{N}$ reaction by means of the $^{17}\text{O}(d, \alpha^{14}\text{N})n$ three body process. Data are reported as black solid dots, with the PWIA distribution as black solid line and the DWBA one as dash-dotted (blue) line. From compari-

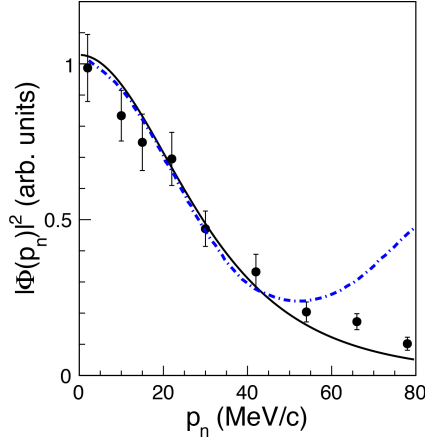


Fig. 2. Experimental momentum distribution from the $^{17}\text{O}(d, \alpha^{14}\text{N})n$ QF reaction (as black solid dots) compared with the theoretical ones: for Plane Wave Impulse Approximation in terms of a Hulthén function (black solid line) and for Distorted Wave Born Approximation evaluated using the FRESKO code (see the dotted (red) line in [52] for further details).

son, one can state that for a neutron momentum $|p_s| \leq 30$ MeV/c, a good agreement between DWBA and PWIA is present. This is a validation that the PWIA approach is viable for the experimental study under investigation and that in the selected kinematical region the QF mechanism gives the main contribution to the $^{17}\text{O} + d$ interaction. Data analysis is usually limited to the region where the agreement between the distributions exists. Usually, a window not more than few tens of MeV/c is chosen, according to the prescriptions of [26]. Therefore, $(d\sigma/d\Omega_{\text{cm}})^{\text{HOES}}$ can be extracted from the three-body coincidence yield by simply inverting Eq. (5). In a final step, the HOES cross section has to be related to the relevant on-energy-shell (OES) cross section by applying the corresponding corrections. In a simple approach, this consists, essentially, in replacing the Coulomb suppression in the HOES cross section, by means of the penetrability factor

$$P_l(k_{Ax}R) = \frac{1}{G_l^2(k_{Ax}R) + F_l^2(k_{Ax}R)} \quad (8)$$

with F_l and G_l regular and irregular Coulomb wave functions. It was demonstrated that there is no Coulomb barrier in the two-body amplitude ex-

tracted from the TH reaction [29] and this is due to the virtuality of particle x . This seems to be the only consequence of off-energy-shell effects as suggested by the agreement between HOES and OES cross sections for the ${}^6\text{Li}(n, \alpha){}^3\text{H}$ reaction [20]. This procedure does not allow us to extract the absolute value of the two-body cross section. However, this is not a real problem since the absolute magnitude can be derived from a scaling to the direct data available at higher energies. Recently, a well assessed THM theory for multi resonance reactions has been developed [29, 48], which allows one to determine the resonance strength in a model independent way. It is called a generalized R-matrix approach as it considers the HOES character of the TH cross section. According to this THM theory for resonant reactions, the resonance strength of the i th resonance, $(\omega\gamma)_i$, is related to the area under each peak, N_i , by easily calculable factors thus ruling out any dependence on the spectroscopic factors

$$(\omega\gamma)_i = \frac{1}{2\pi} \omega_i N_i \frac{\Gamma_{Ax}}{\frac{d\sigma_{A(a,c)C}}{d\Omega_n}} \quad (9)$$

with $\frac{d\sigma_{A(a,c)C}}{d\Omega_n}$ the transfer reaction differential cross section taken in the Distorted Wave Born Approximation form as reported in [48]. The spectroscopic factor for the i th resonance does not appear because it cancels out in the $\frac{\Gamma_{Ax}}{d\sigma_{A(a,c)C}/d\Omega_n}$ ratio, both involved factors being proportional to it.

3. Recent results

The THM has been applied to many charged particle reactions involved in the Big Bang and stellar elemental nucleosynthesis [30]. A list of them is given in Table I together with the relevant references. A number of reactions belonging to the nucleosynthesis path of ${}^{19}\text{F}$ in Asymptotic Giant Branch (AGB) stars, have been recently investigated using the THM. In spite of being the less abundant among the stable nuclides with mass number $12 \leq A \leq 22$, its abundance can be used to constrain AGB models as it is sensitive to the efficiency of the dredge-up and to the physical conditions in the deep layers of the stars (Lugaro *et al.* 2004). When the abundances predicted by the current models are compared with the observed ones, an unacceptable discrepancy shows up even when model parameters are varied in a reasonable range. A possible explanation can be found in a redetermination of the nuclear reaction rates involved in the fluorine production and destruction. Some of them are affected by large uncertainties mainly due to the fact that they are dominated by the strengths of low-lying resonances, whose resonance parameters are far from being well determined. In addition, the presence of low-lying resonances prevents any extrapolation procedure to be reliable. This is the case of the ${}^{19}\text{F}(p, \alpha_0){}^{16}\text{O}$ reaction, the

TABLE I

Two-body reactions studied via the THM with measured two-to-three TH reaction and relevant references for each reaction.

Direct reaction	TH reaction	Ref.
${}^7\text{Li}(p, \alpha){}^4\text{He}$	${}^7\text{Li}(d, \alpha \alpha)n$	[19]
${}^7\text{Li}(p, \alpha){}^4\text{He}$	${}^7\text{Li}({}^3\text{He}, \alpha \alpha){}^2\text{H}$	[22]
${}^6\text{Li}(d, \alpha){}^4\text{He}$	${}^6\text{Li}({}^6\text{Li}, \alpha \alpha){}^4\text{He}$	[31]
${}^6\text{Li}(p, \alpha){}^3\text{He}$	${}^6\text{Li}(d, \alpha {}^3\text{He})n$	[32]
${}^{11}\text{B}(p, \alpha){}^8\text{Be}$	${}^{11}\text{B}(d, {}^8\text{Be} \alpha)n$	[39]
${}^{10}\text{B}(p, \alpha){}^7\text{Be}$	${}^{10}\text{B}(d, {}^7\text{Be} \alpha)n$	[40, 41]
${}^9\text{Be}(p, \alpha){}^6\text{Li}$	${}^9\text{Be}(d, {}^6\text{Li} \alpha)n$	[42, 43]
${}^2\text{H}({}^3\text{He}, p){}^4\text{He}$	${}^6\text{Li}({}^3\text{He}, p \alpha){}^4\text{He}$	[44]
${}^2\text{H}(d, p){}^3\text{H}$	${}^2\text{H}({}^6\text{Li}, t p){}^4\text{He}$	[45]
${}^{15}\text{N}(p, \alpha){}^{12}\text{C}$	${}^{15}\text{N}(p, \alpha){}^{12}\text{C}n$	[46]
${}^{18}\text{O}(p, \alpha){}^{15}\text{N}$	${}^{18}\text{O}(p, \alpha){}^{15}\text{N}n$	[47, 48]
${}^1\text{H}(p, p){}^1\text{H}$	${}^2\text{H}(p, pp)n$	[15, 16]
${}^2\text{H}(d, p){}^3\text{H}$	${}^2\text{H}({}^3\text{He}, t p){}^1\text{H}$	[49, 50]
${}^2\text{H}(d, n){}^3\text{He}$	${}^2\text{H}({}^3\text{He}, {}^3\text{He} n){}^1\text{H}$	[49, 50]
${}^{19}\text{F}(p, \alpha){}^{16}\text{O}$	${}^2\text{H}({}^{19}\text{F}, \alpha){}^{16}\text{O}n$	[51]
${}^{17}\text{O}(p, \alpha){}^{14}\text{N}$	${}^2\text{H}({}^{17}\text{O}, \alpha){}^{14}\text{N}n$	[52]
${}^4\text{He}({}^{12}\text{C}, {}^{12}\text{C}){}^4\text{He}$	${}^6\text{Li}({}^{12}\text{C}, \alpha){}^{12}\text{C}{}^2\text{H}$	[53]
$n({}^6\text{Li}, t){}^4\text{He}$	${}^2\text{H}({}^6\text{Li}, t {}^4\text{He}){}^1\text{H}$	[20, 21]
${}^{11}\text{B}(p, \alpha){}^8\text{Be}$	${}^2\text{H}({}^{11}\text{B}, \alpha){}^8\text{Be}n$	[54]
${}^{13}\text{C}(\alpha, n){}^{16}\text{O}$	${}^6\text{Li}({}^{13}\text{C}, n){}^{16}\text{O}{}^2\text{H}$	[55]

main ${}^{19}\text{F}$ destruction channel in the range of temperatures $0.01 \leq T_9 \leq 0.1$, with $T_9 = T/10^9$ K, where T is the temperature of the astrophysical site. Available experimental data have allowed the computation of the rate for $T_9 \geq 0.3$. Below this temperature, the rate was determined mainly from the non-resonant (p, α_0) channel, causing an increase of the uncertainties up to 50% at the lowest temperatures. To determine the contribution of low-lying resonances at astrophysical energies and evaluate their impact on astrophysics, the ${}^{19}\text{F}(p, \alpha_0){}^{16}\text{O}$ astrophysical $S(E)$ -factor has been measured by means of the THM applied to the ${}^2\text{H}({}^{19}\text{F}, \alpha_0){}^{16}\text{O}n$ reaction at 50 MeV of beam energy. The normalized coincidence yield of the ${}^2\text{H}({}^{19}\text{F}, \alpha_0){}^{16}\text{O}n$ reaction shows several peaks, corresponding to the population of a number of states of ${}^{20}\text{Ne}$ at 12.96, 13.05, 13.25 (three not resolved states at 13.222, 13.224 and 13.226 are contributing to this peak) and 13.6 (also here three not resolved states at 13.529, 13.586 and 13.642 contribute). For a detailed analysis, see [51]. The OES $S(E)$ -factor resulting from the R-matrix pa-

parameterization using the γ_p and γ_{α_0} from [51] is shown in Fig. 3. Above 0.6 MeV, the reduced partial widths were obtained through an R-matrix fit of direct data (solid black dots and squares data from [59] and [60] respectively). Since the TH cross section gives the resonance contribution only,

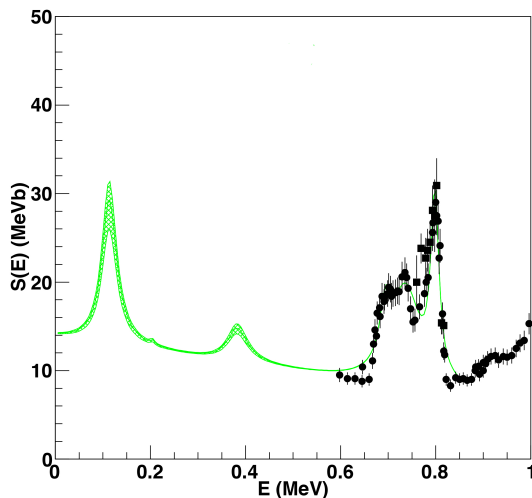


Fig. 3. R-matrix parameterization of the $^{19}\text{F}(p, \alpha_0)^{16}\text{O}$ $S(E)$ -factor (grey/green line). The grey/green band shows the region allowed by the uncertainties on the fitting parameters. Black symbols represent direct data from [59] (circles) and [60] (squares).

the non-resonant part of the cross section was taken from Angulo *et al.* 1999. The middle grey/green curve represents the $S(E)$ -factor obtained using the parameters from the best fit, while the grey/green band arises from the uncertainties in the resonance parameters of the 12.957, 13.048, 13.222, 13.224, and 13.226 MeV ^{20}Ne states (see [51] for details). The main result of the present work is the estimate of the contribution of the 12.957 MeV level of ^{20}Ne to the total astrophysical factor, as it is associated to a resonance at 113 keV, well inside the energy range of astrophysical interest. The energy resolution was not enough for achieving a good separation between resonances around a ^{19}F - p relative-energy of 400 keV, thus preventing an accurate estimate of their total widths. Thus, the interesting results already achieved call for improved investigations in the full energy region with a better energy resolution to perform more accurate spectroscopy of the involved resonances.

Another interesting reaction that has been investigated using the THM is the $^{17}\text{O}(p, \alpha)^{14}\text{N}$ that plays a key role in novae nucleosynthesis and in γ -ray astronomy. ^{17}O is processed in the CNO cycles and it is important

for the subsequent formation of the short-lived ^{18}F radioisotope, of special interest in novae observations in the γ -ray wavelengths. The cross section of the $^{17}\text{O}(p, \alpha)^{14}\text{N}$ reaction at low energy is dominated by two resonances at ^{17}O - p relative energies of 65 keV and 183 keV, whose strengths are still quite uncertain due to the strong Coulomb suppression at those energies. For this reason, the study of the $^{17}\text{O}(p, \alpha)^{14}\text{N}$ reaction at low-energies was performed by means of the THM applied to the $^2\text{H}(^{17}\text{O}, \alpha^{14}\text{N})n$ reaction [7]. The resulting $^{17}\text{O}(p, \alpha)^{14}\text{N}$ cross section is shown in Fig. 4 as black solid dots. The solid (black) line represents the fit of the two-body cross section using three Gaussian functions (dashed (blue) lines) to describe the resonant behavior (which account for the finite energy resolution of the detectors) and a straight line (dash-dotted (blue) line) to account for the non-resonant contribution to the cross section. This analysis does not take into account interference effects since the natural widths of the resonances (eV) are much smaller than their energy separation (keV). Because of the energy resolution (20 keV), the resonance at 65 keV was not well separated from the high energy tail of the -3 keV sub-threshold state, corresponding to the 5.603 MeV level of ^{18}F . The sub-threshold as well as the non-resonant contributions were evaluated so that the experimental TH angular distributions for the 183 keV resonance were in agreement with the experimental ones [56] and with the theoretical prediction for both the 65 keV and the 183 keV resonances based on the general theory reported in [57]. The resulting TH strength of the 65 keV resonance was used to calculate its contribution to the total reaction

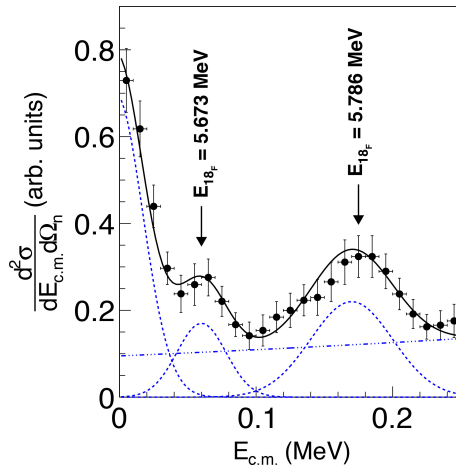


Fig. 4. Cross section of the TH reaction (solid (black) dots). The full line represents the result of a fit including three Gaussian curves (dashed (blue) lines) and a 1st order polynomial (dash-dotted (blue) line) to take into account the non-resonant contribution to the cross section.

rate providing a 20% decrease when compared with previous estimates as reported in [56]. A possible explanation of such discrepancy can be found in the electron screening effect that was not taken into account in the direct measurement [58]. When a reaction cross section is dominated by narrow resonances, as in the present case, the electron screening correction depends on the relative magnitude of the incoming and outgoing partial widths and its theoretical treatment is more complicated than in “non-resonance”/“broad resonance” case. Further work in this sense is presently being undertaken.

This work was supported in part by the Italian Ministry of Education, University and Research under Grant ASTROF.NUC.MIUR/0000.

REFERENCES

- [1] E.M. Burbige *et al.*, *Rev. Mod. Phys.* **29**, 547 (1957).
- [2] C. Rolfs, W.S. Rodney, *Caldrons in the Cosmos*, Univ. of Chicago Press, Chicago 1988.
- [3] C. Rolfs, *Prog. Part. Nucl. Phys.* **46**, 23 (2001).
- [4] H. Assenbaum *et al.*, *Z. Phys.* **A327**, 461 (1987).
- [5] A. Tumino *et al.*, *Few Body Syst.* **54**, 869 (2013).
- [6] G. Baur, C. Bertulani, H. Rebel, *Nucl. Phys.* **A458**, 188 (1986).
- [7] A.M. Mukhamedzhanov, R.E. Tribble, *Phys. Rev.* **C59**, 3418 (1999).
- [8] G. Baur, *Phys. Lett.* **B178**, 135 (1986).
- [9] C. Spitaleri *et al.*, *Phys. Rev.* **C60**, 055802 (1999).
- [10] C. Spitaleri *et al.*, *Nucl. Phys.* **A719**, 99c (2003).
- [11] S. Typel, H. Wolter, *Few Body Syst.* **29**, 7 (2000).
- [12] A.M. Mukamedzhanov *et al.*, *J. Phys. G: Nucl. Part. Phys.* **35**, 014015 (2008).
- [13] C. Spitaleri *et al.*, *Phys. At. Nucl.* **74**, 1725 (2011).
- [14] A. Tumino *et al.*, *Few Body Syst.* **54**, 745 (2013).
- [15] A. Tumino *et al.*, *Phys. Rev. Lett.* **98**, 252502 (2007).
- [16] A. Tumino *et al.*, *Phys. Rev.* **C68**, 064001 (2008).
- [17] M. Lattuada *et al.*, *Nucl. Phys.* **A458**, 493 (1985).
- [18] M. Zadro *et al.*, *Phys. Rev.* **C40**, 181 (1989).
- [19] M. Lattuada *et al.*, *Astrophys. J.* **562**, 1076 (2001).
- [20] A. Tumino *et al.*, *Eur. Phys. J.* **A25**, 649 (2005).
- [21] M. Gulino *et al.*, *J. Phys. G: Nucl. Part. Phys.* **37**, 125105 (2010).
- [22] A. Tumino *et al.*, *Eur. Phys. J.* **A27**, 243 (2006).
- [23] R.G. Pizzone *et al.*, *Phys. Rev.* **C83**, 045801 (2011).

- [24] R.G. Pizzone *et al.*, *Phys. Rev.* **C71**, 058801 (2005).
- [25] R.G. Pizzone *et al.*, *Phys. Rev.* **C87**, 025805 (2013).
- [26] I.S. Shapiro, V.M. Kolybasov, J.P. August, *Nucl. Phys.* **61**, 353 (1965).
- [27] I.J. Thompson, *Comput. Phys. Rep.* **7**, 167 (1987).
- [28] C.M. Perey, F.G. Perey, *At. Data Nucl. Data Tables* **17**, 1 (1976).
- [29] A.M. Mukhamedzhanov *et al.*, *Eur. Phys. J.* **A27**, 205 (2006).
- [30] C.J. Copi, D.N. Schramm, M.S. Turner, *Science* **267**, 192 (1995).
- [31] C. Spitaleri *et al.*, *Phys. Rev.* **C63**, 055801 (2001).
- [32] A. Tumino *et al.*, *Phys. Rev.* **C67**, 065803 (2003).
- [33] A. Tumino *et al.*, *Prog. Theor. Phys. Suppl.* **154**, 341 (2004).
- [34] M. Aliotta *et al.*, *Eur. Phys. J.* **A9**, 435 (2000).
- [35] R.G. Pizzone *et al.*, *Astron. Astrophys.* **398**, 423 (2003).
- [36] L. Lamia *et al.*, *Astron. Astrophys.* **541**, A158 (2012).
- [37] R.G. Pizzone *et al.*, *Astron. Astrophys.* **438**, 779 (2005).
- [38] L. Lamia *et al.*, *Astrophys. J.* **768**, 65 (2013).
- [39] C. Spitaleri *et al.*, *Phys. Rev.* **C69**, 055806 (2004).
- [40] L. Lamia *et al.*, *Nucl. Phys.* **A787**, 309 (2007).
- [41] L. Lamia, *et al.*, *Il Nuovo Cim.* **C31**, 423 (2008).
- [42] Qun-Gang Wen *et al.*, *Phys. Rev.* **C78**, 035805 (2008).
- [43] Qun-Gang Wen *et al.*, *J. Phys. G: Nucl. Part. Phys.* **38**, 085103 (2011).
- [44] M. La Cognata *et al.*, *Eur. Phys. J.* **A27**, 249 (2006).
- [45] A. Rinollo *et al.*, *Nucl. Phys.* **A758**, 146 (2005).
- [46] M. La Cognata *et al.*, *Phys. Rev.* **C76**, 065804 (2007).
- [47] M. La Cognata *et al.*, *Phys. Rev. Lett.* **101**, 152501 (2008).
- [48] M. La Cognata *et al.*, *Astrophys. J.* **708**, 796 (2010).
- [49] A. Tumino *et al.*, *Phys. Lett.* **B700**, 111 (2011).
- [50] A. Tumino *et al.*, *Phys. Lett.* **B705**, 546 (2011).
- [51] M. La Cognata *et al.*, *Astrophys. J. Lett.* **739**, L54 (2011).
- [52] M.L. Sergi *et al.*, *Phys. Rev.* **C82**, 032801(R) (2010).
- [53] C. Spitaleri *et al.*, *Eur. Phys. J.* **A7**, 181 (2000).
- [54] L. Lamia *et al.*, *J. Phys. G: Nucl. Part. Phys.* **39**, 015106 (2012).
- [55] M. La Cognata *et al.*, *Phys. Rev. Lett.* **49**, 015106 (2013).
- [56] A. Chafa *et al.*, *Phys. Rev.* **C75**, 035810 (2007).
- [57] J.M. Blatt, L.C. Biedenharn, *Rev. Mod. Phys.* **24**, 258 (1952).
- [58] J.C. Blackmon *et al.*, *Phys. Rev. Lett.* **74**, 2642 (1995).
- [59] A. Isoya *et al.*, *Nucl. Phys.* **7**, 116 (1958).
- [60] R. Caracciolo *et al.*, *Lett. Nuovo Cim.* **11**, 33 (1974).